ISSN 1070-3284, Russian Journal of Coordination Chemistry, 2024, Vol. 50, No. 5, pp. 316–325. © Pleiades Publishing, Ltd., 2024.

Isonitrile Coordination to Pincer Iridium Hydrido Chlorides

E. S. Gulyaeva[a], E. I. Gutsul[a], Y. V. Nelyubina[a, b], E. S. Osipova[a], O. A. Filippov[a], E. S. Shubina[a], and N. V. Belkova[a, *]

[a] *. Nesmeyanov Institute of Organoelement Compounds of Russian Academy of Sciences, Moscow, Russia*
[b] *Moscow Institute of Physics and Technology (National Research University), Moscow oblast, Russia*
**e-mail: nataliabelk@ineos.ac.ru*

Received December 5, 2023; revised February 5, 2024; accepted February 5, 2024

Abstract—Isonitriles are useful reagents that participate in many cycloaddition or multicomponent reactions of interest in organic synthesis, which are often catalyzed by transition metal complexes. Being good electron donors, RN=C bonds become activated and prone to the nuclephilic attack upon coordination to electrophilic (Lewis acidic) metal centers. Herein we explore the complexation of ^{t}BuNC to a series of iridium hydrido chlorides supported by benzene-based pincer ligands, (R-$^{t\text{Bu}}$PZCZP)IrH(Cl) (R-$^{t\text{Bu}}$PZCZP = κ^3-C_6H_3–2,6-(ZP^{t}Bu$_2$)$_2$, where R = H (**I**–**III**), EtCO$_2$–(**IV**), and Z = CH$_2$ (**I**), CH$_2$, O (**II**), O (**III**, **IV**)), that occurs instantaneously and quantitatively in solution yielding one of possible isomers **Ia**–**IVa**. Single crystal X-ray diffraction studies for **Ia**–**IIIa** confirmed the apical coordination of isonitrile ligand *trans* to hydride ligand suggested by NMR studies. Perusal of the structural data suggests stronger binding of ^{t}BuNC to PCP-supported iridium center in complex **Ia** in comparison to PCOP/POCOP species **IIa**–**IIIa**. Structural data also reveal a distortion in the P–Ir–P arrangement caused by ^{t}BuNC docking in apical position that is the most noticeable for asymmetric PCOP version **IIa**. The computational analysis of vibrational frequencies unveils an essential coupling $\nu_{Ir\text{-}H}$ and $\nu_{N=C}$ modes that produce two strong bands of similar intensity in the $\nu_{N=C}$ region for **Ia**. Weaker isonitrile binding in **IIa**–**IVa** with shorter N=C and longer N–C$^{t\text{Bu}}$/Ir–C$_{CN}$ bonds and a plethora of intramolecular interactions result in a different degree of vibrational mixing for Ir–H and N=C stretches as well as lead to an intense bands due to a Fermi resonance of low frequency modes involving vibrations of N–C–^{t}Bu fragment. Thus, the raw experimental IR data should be taken with care as an indicator of RN=C activation, paying attention to the vibrational coupling. An estimation of band position for the "true" (uncoupled) ν_{NC} vibration gives a small high frequency shift for **Ia** (+16 cm^{-1}) but low frequency shifts for other complexes becoming less negative in the order **IIa**–**IIa**–**IVa** (PCOP–POCOP–EtCO$_2$-POCOP). Overall the results obtained show the influence of the pincer ligand on the complex picture of isonitrile complexes structure and spectra, and suggest that strong binding does not always mean a strong activation.

Keywords: *tert*-butylisonitrile, pincer complexes, iridium, X-ray diffraction, IR spectroscopy, vibrational coupling

DOI: 10.1134/S1070328423601541

INTRODUCTION

Pincer metal complexes continue to receive attention due to their amenable modularity that allows the development of very successful catalysts [1–6]. The meridional coordination of tridentate pincer ligands provides a high thermal stability to the resulting metal complexes that is important for their catalytic efficacy in strongly endothermic reactions [2, 7, 8]. Iridium pincer species are perceived as efficient catalysts for alkanes dehydrogenation of alkanes and aliphatic groups that operate under much milder conditions than those required for the heterogeneous catalyst [9–11]. Among them those of the form (^{R}PZCZP)IrX$_n$ (^{R}PZCZP = κ^3-C_6H_3–2,6-(ZPR$_2$)$_2$, where Z = CH$_2$, O, and X = H, Cl, n = 2, 4) are explored the most often showing the activity not only in dehydrogenation of alkanes but also amines [12], aminoborane [13], and even N-ethyl perhydrocarbazole [10], which are considered as liquid organic hydrogen carriers. These studies demonstrated the electronic environment of the metal center and the catalytic performance of the pincer complex is highly sensitive to minor changes in the pincer ligand. Such modulation can be achieved by changing R substituents at phosphorus, variation of Z bridges or introduction of electron donating/accepting group into aromatic ring of pincer ligand.

An important structural feature of the catalytically active (^{R}PZCZP)IrH_2 dihydride complexes and their hydridochloride precursors is the pentacoordinate geometry of the metal center. According to the XRD analysis, hydridochloride complexes have a square-pyramidal geometry, where the hydride occupies an apical position, and the donor atoms of the pincer ligand and chloride substituent form the base plane of the pyramid [14] with a local MEP maximum located at the empty coordination place and coinciding with the LUMO location [14, 15]. The same pattern was found for corresponding dihydrides [14, 15], thereby this might be expected as a site for coordination of a substrate or an additional ligand, however that is not always the case. Thus, bubbling CO through a ($^{t\text{Bu}}$PCP)IrH(Cl) (**I**) solution gives hexacoordinated **I**·CO complex, in which the carbonyl ligand is in *trans* position to the hydride ligand [16]. On a contrary, in crystals of the hexacoordinate complexes of **I** with pyridine (Py) and 4-aminopyridine (4APy), the pyridine molecule is coordinated equatorially (in *trans* position to the aromatic ring of the pincer ligand) [17]. At the same time, variable temperature NMR and UV-vis spectroscopic studies showed the energetic (enthalpic) preference of apical coordination of nitrogen bases (PhCN or Py) resulting in the dominance of apical isomers in solution [14, 15, 17] in agreement with the DFT calculations [15, 18]. The experimentally determined stability of these apical isomers changes in the order: ($^{t\text{Bu}}$PCP)IrH(Cl)(L) > (EtCOO-$^{t\text{Bu}}$POCOP)IrH(Cl)(L) > ($^{t\text{Bu}}$POCOP)-IrH(Cl)(L), with the $\Delta H°$ values varying from −17 to −5 kcal/mol for L = MeCN, PhCN [15]. In this work we study the interaction of *tert*-butylisonitrile with a series of hydridochloride complexes ($^{t\text{Bu}}$PZCZP)IrH(Cl) (Scheme 1) aiming to estimate the influence of the pincer scaffold on the properties of the C=N bond as a model unsaturated substrate. It is well established, that isonitriles ligating electron-poor metal centers can undergo α-nucleophilic addition to afford either heterocyclic or acyclic aminocarbene ligands [19, 20]. However, the resulting metal–carbene bonds are very stable toward further reactions, and the complexes obtained are rather utilized in asymmetric catalysis or materials science than as catalysts for aminocarbene synthesis through nucleophilic addition to isonitriles [21].

EXPERIMENTAL

All synthetic work was performed under a purified argon atmosphere using standard Schlenk techniques. CH_2Cl_2 was stored over CaH_2 and distilled under the inert atmosphere of argon prior to use. Deuterated solvents for NMR spectroscopy were degassed before use by three freeze-pump-thaw cycles and kept over 4 Å molecular sieves. The ligands and iridium compounds ($^{t\text{Bu}}$PCP)IrH(Cl) (**I**), ($^{t\text{Bu}}$PCOP)IrH(Cl) (**II**), ($^{t\text{Bu}}$POCOP)IrH(Cl) (**III**) and (EtCO$_2$-$^{t\text{Bu}}$POCOP)IrH(Cl) (**IV**) were synthesized following the methods described in the literature [22–25]. Reagent grade ^{t}BuNC was used without additional purification.

^{1}H, ^{31}P{^{1}H} NMR spectra were recorded on a Bruker Avance400 spectrometer. The resonances were calibrated relative to the residual solvent peaks (^{1}H) or referred to external 85% H_3PO_4 (^{31}P). IR spectra of solutions were measured in 0.05 or 0.2 cm CaF_2 cells on Nicolet iS50 spectrometer and are given in cm^{-1} with relative intensity in parenthesis. Thin films of **I**–**IV** and **Ia**–**IVa** were prepared from CH_2Cl_2 solutions (c = 0.008 M) of corresponding complexes upon evaporation of solvent on CaF_2 plates. Various temperatures (190–293 K) IR spectra were recorded using a home-modified cryostat (Carl Zeiss Jena). The accuracy of the experimental temperature adjustment was ±0.5°C. Elemental analysis was performed at the Laboratory of Microanalysis of INEOS RAS.

Synthesis of complexes Ia–IVa. Starting compounds **I**–**IV** (0.150 mmol, ca. 100 mg) was dissolved in dichloromethane (4 mL) giving an orange or red solution. Then 1.05 equiv. of *tert*-butylisonitrile (0.225 mmol, 25.5 μL) was added by microsyringe producing colorless solutions of **Ia**–**IVa**. The solvent was removed under reduced pressure and the residue was dried in vacuum at room temperature for 8 h to eliminate traces of *tert*-butylisonitrile and obtain the target complexes as white powders with quantitative yields (ca. 99%).

($^{t\text{Bu}}$PCP)IrH(Cl)(CN^{t}Bu) (Ia). ^{1}H NMR (400.13 MHz, CD_2Cl_2, 294 K): 6.77 (d, 2H J_{HH} = 7.3 Hz, *m*-HAr), 6.61 (t, 1H, J_{HH} = 7.4 Hz, *p*-HAr), 3.21 (s, 4H, CH_2), 1.46 (t, 18H J_{HP} = 6.6 Hz, −P(^{t}Bu)$_2$), 1.31 (s, 9H, CN^{t}Bu), 1.28 (t, 18H, J_{HP} = 6.6 Hz, −P(^{t}Bu)$_2$), −10.61 (t, 1H, J_{HP} = 16.2 Hz, IrH). ^{31}P{^{1}H} NMR (121.51 MHz, CD_2Cl_2, 294 K): 54.11 (s, −P(^{t}Bu)$_2$). IR (thin film, CaF_2): ν_{NC} 2183 (s), 2123 (s).

($^{t\text{Bu}}$PCOP)IrH(Cl)(CN^{t}Bu) (IIa). ^{1}H NMR (400.13 MHz, CD_2Cl_2, 294 K): 6.68 (m, 2H, *m*-HAr) 6.64 (m, 1H, *p*-HAr), 3.14 (m, 1H, CH_2), 2.96 (m, 1H, CH_2), 1.11–1.52 (m, 36H, −P(^{t}Bu)$_2$), 0.84 (s, 9H, CN^{t}Bu), −10.74 (dd, 1H, J_{HP} = 14.00 Hz, J_{HP2} = 18.40 Hz, IrH). ^{31}P{^{1}H} NMR (121.51 MHz, CD_2Cl_2, 294 K): 51.52 (d, J_{PP} = 335.75 Hz, −CH_2P(^{t}Bu)$_2$),

161.07 (d, J_{PP} = 335.75 Hz, $-OP(^tBu)_2$). IR (thin film, CaF_2): ν_{NC} 2123 (s), 2100 (s).

$C_{28}H_{51}ClIrNOP_2$ (M_r = 707.28)

Anal. calcd.,% C, 47.55 H, 7.27 Cl, 5.01 Ir, 27.17 N, 1.98 O, 2.26 P, 8.76
Found, % C, 47.48 H, 7.21 N, 1.97

($^{t\text{Bu}}$POCOP)IrH(Cl)(CN^{t}Bu) (IIIa). ^{1}H NMR (300.00 MHz, CD_2Cl_2, 294 K): 6.67 (t, 1H, J_{HH} = 7.83 Hz, *p*-HAr) 6.39 (d, 2H, J_{HH} = 7.83 Hz, *m*-HAr), 1.54 (t, 18H, J_{HP} = 7.02 Hz, $-OP(^tBu)_2$), 1.46 (s, 9H, CN^{t}Bu), 1.38 (t, 18H, J_{HP} = 7.02 Hz, $-OP(^tBu)_2$), −11.34 (t, 1H, J_{HP} = 16.14 Hz, Ir<u>H</u>). $^{31}P\{^1H\}$ NMR (121.51 MHz, CD_2Cl_2, 294 K): 161.21 (s, $-OP(^tBu)_2$). IR (thin film, CaF_2): ν_{NC} 2145 (s), 2110 (s).

$C_{27}H_{49}ClIrNO_2P_2$ (M_r = 709.26)

Anal. calcd.,% C, 45.72 H, 6.96 Cl, 5.00 Ir, 27.10 N, 1.97 O, 4.51 P, 8.73
Found, % C, 45.79 H, 6.81 N, 2.02

(EtCO$_2$-$^{t\text{Bu}}$POCOP)IrH(Cl)(CN^{t}Bu) (IVa). ^{1}H NMR (300.00 MHz, CD_2Cl_2, 294 K): 7.02 (s, 2H, *m*-HAr), 4.24 (q, 2H, *J* = 7.1 Hz, $-CH_2-$), 1.51 (t, 18H, *J* = 7.2 Hz, $-OP(^tBu)_2$), 1.42 (s, 9H, CN^{t}Bu), 1.35 (t, 18H, J_{HP} = 7.5 Hz, $-OP(^tBu)_2$), 1.3 (3H, $-CH_3$, overlapped with ^{t}Bu group), −11.30 (t, 1H, J_{HP} = 16.3 Hz, IrH). $^{31}P\{^1H\}$ NMR (121.51 MHz, CD_2Cl_2, 294 K): 162.3 (s, $P(^tBu)_2$). IR (thin film, CaF_2): ν_{NC} 2148 (s), 2114 (s).

IR spectra. 1. *Variable temperatures IR monitoring*. The solutions of **I**–**IV** (*c* = 0.02 M) were prepared at room temperature in 2 mL of CH_2Cl_2, and then were cannulated under an inert atmosphere into the cryostat at 290 K. After the acquisition of reference IR spectrum of initial complex, the solution was removed from the cryostat to the Schlenk tube and 1 equiv. of ^{t}BuNC (0.04 mmol, 4.6 μL) was added at room temperature. The resulting mixture was quickly mixed, returned into the cryostat and monitored by IR spectroscopy in the 190–290 K temperature range.

2. *Room temperature ^{t}BuNC titration*. The solution of ^{t}BuNC (*c* = 0.04 M) was prepared at room temperature in 0.7 mL of CH_2Cl_2. The aliquot was taken with a Pasteur pipette and placed in the inert gas filled cell (*l* = 0.05 cm) and then removed back into the Schlenk tube after the reference IR spectrum acquisition. Then 0.2 equiv. of solid complex **I** (0.0056 mmol, 3.5 mg) was added in an inert gas flow. Obtained mixture was quickly mixed until **I** was completely dissolved, and an aliquot was transferred in the inert gas filled cell to acquire an IR spectrum at room temperature. Then the aliquot was removed back into the Schlenk tube and another 0.2 equiv. of **I** (0.0056 mmol, 3.5 mg) were added. The procedure was repeated until the overall amount of added was 1 equiv. of **I** (0.028 mmol, 17.5 mg).

NMR spectra. The solution of **I**–**IV** (*c* = 0.02 M) was prepared at room temperature (~25°C) in 0.5 mL of CD_2Cl_2 and transferred to NMR tube under inert atmosphere, and the reference NMR spectra of initial complex was acquired at room temperature. Then 1 equiv. of ^{t}BuNC (0.01 mmol, 1.1 μL) was added at room temperature. The resulting solution was quickly mixed until complete discoloration of initially red-colored solution, and the tube was placed into NMR spectrometer to acquire the spectra at room temperature.

X-ray crystallography. X-ray diffraction data for **Ia**–**IIIa** were collected on a Bruker APEX2 DUO CCD diffractometer, using graphite monochromated MoK_α radiation (λ = 0.71073 Å, ω-scan) at 120 K. Structures were solved using Intrinsic Phasing with the ShelXT [26] structure solution program in Olex2 [27] and then refined with the XL refinement package [28] using Least-Squares minimization against F^2 in the anisotropic approximation for non-hydrogen atoms. Hydrogen atoms at the metal centers were found in difference Fourier synthesis while positions of others were calculated, and they all were refined in the isotropic approximation within the riding model. Crystal data and structure refinement parameters are given in Table 1.

Crystallographic data for structures **Ia**, **IIa**, **IIIa** have been deposited with the Cambridge Crystallographic Data Centre (CCDC nos. 2282336, 2282337, and 2282335, respectively; www.ccdc.cam.ac.uk/data_request/cif).

DFT calculations were performed with the Gaussian09 [29] package at the DFT/M06 [30] (method 1) or B3PW91 [31, 32] (method 2) level without any ligand simplification. The basis set for method **1** was inherited from our previous works [14, 15, 18, 33–36] and contain effective core potentials (ECP) and its associated SDD basis set [37–40] supplemented with f-polarization functions (SDD(f)) [41] for the Ir atom, 6-31++G(d,p) basis set [42–45] for carbon atoms of benzene ring, P atoms, H and Cl ligands, as well as all atoms of the ^{t}BuNC ligand; ^{t}Bu groups of PCP was described with a 6-31G basis set [42]. Basis set for method 1 was def2-TZVP [46] for all atoms, supplied with ECP for Ir atom [47]. The structure of complex **Ia** was fully optimized with these methods without any symmetry restrictions. Frequencies were calculated at found stationary points and reported without any scaling factors.

RESULTS AND DISCUSSION

The coordination of *tert*-butylisonitrile to complexes **I**–**IV** proceeds instantly already at room tem-

Table 1. Crystal data and structure refinement parameters for **Ia**–**IIIa**

Parameter	Value		
	Ia	**IIa**	**IIIa**
Empirical formula	$C_{29}H_{53}NP_2ClIr$	$C_{28}H_{51}NOP_2ClIr$	$C_{27}H_{49}NO_2P_2ClIr$
M	705.31	707.28	709.26
T, K	120	120	120
Crystal system	Orthorhombic	Orthorhombic	Tetragonal
Space group	*Pbcn*	$P2_12_12_1$	$P\text{-}42_1c$
Z	8	4	8
a, Å	33.7754(17)	11.0316(4)	17.1435(11)
b, Å	16.5493(8)	11.3712(5)	17.1435(11)
c, Å	11.3301(6)	24.0057(10)	20.8599(13)
α, deg	90	90	90
β, deg	90	90	90
γ, deg	90	90	90
V, Å^3	6333.1(6)	3011.3(2)	6130.7(9)
ρ_{calcd}, g cm^{-3}	1.479	1.560	1.537
μ, cm^{-1}	44.19	46.5	45.7
F(000)	2864	1432	2864
θ_{max}, deg	52	54	54
Number of measured reflections	110056	53647	64308
Number of independent reflections	6221	6581	6702
Observed reflections ($I > 2\sigma(I)$)	4779	6225	5598
Parameters	326	327	327
R_1 ($F^2 > 2\sigma(F^2)$)	0.0364	0.0214	0.0351
wR_2 (all data)	0.0797	0.0454	0.0677
$S(F^2)$	1.091	1.059	1.021
Residual electron density (max/min), e Å^{-3}	1.082/−2.238	1.427/−0.373	1.249/−1.049

perature, yielding quantitatively the hexacoordinate products **Ia**–**IVa** (Scheme 1). This reaction is accompanied by discoloration of initially red-colored solutions. No starting material was observed in IR and NMR spectra of equimolar reagents mixtures in dichloromethane. Inspection of variable temperature ^{1}H and ^{31}P{^{1}H} spectra reveals that complexes **Ia**–**IVa** exist in one isomeric form (Table 2) those sharp signals do not show any dynamic behavior. Single crystal X-ray diffraction study for complexes **Ia**–**IIIa** showed they have same configuration with apical coordination of ^{t}BuNC (Fig. 1) These hexacoordinate complexes have never been characterized; the closest analogues found in the Cambridge Structural Database (CSD) bearing the same ^{tBu}PCP-pincer ligand are represented by (PCP)IrH(CN^{t}Bu) scaffold with $-NH_2$ [48], $-CH_2NO_2$ [49], or $-CH_3$ [50] ligands. The later complex, (PCP)IrH(CH_3)(CN^{t}Bu), was crystalized as equatorial isomer with isonitrile ligand *trans* to benzene ring. Similar geometry has been reported for (PCP)Ir-based dihydrides coordinating MeNC or PhNC moieties [51].

Table 2. Selected NMR (chemical shifts in ppm, spin-spin coupling constants $^2J_{PH}$ in Hz in CD_2Cl_2 at 298 K) and IR (band positions, in cm^{-1} for thin films) parameters for the complexes with *tert*-butylisonitrile **Ia**–**IVa**

	^1H ($^2J_{PH}$)	$\Delta\delta_H$	$^{31}P\{^1H\}$	ν_1, cm^{-1}	ν_2, cm^{-1}
(PCP)IrH(Cl)(CN^{t}Bu) (**Ia**)	−10.54 (*16.3*)	32.13	54.32	2182	2120
(PCOP)IrH(Cl)(CN^{t}Bu) (**IIa**)	−10.74 (*14.0*, *18.4*)	30.55	160.43, 50.94 (*335.8*)*	2133	2100
(POCOP)IrH(Cl)(CN^{t}Bu) (**IIIa**)	−11.38 (*16.2*)	30.07	162.22	2145	2110
($EtCO_2$–POCOP)IrH(Cl)(CN^{t}Bu) (**IVa**)	−11.22 (*15.7*)		163.16	2148	2114

* $^2J_{P(1)P(2)}$.

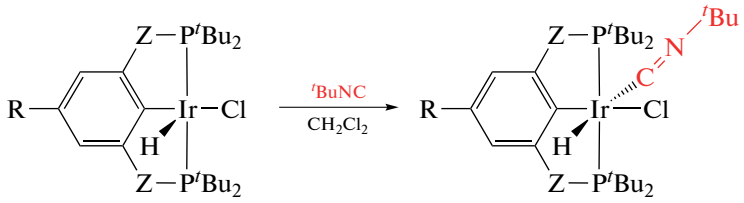

I Z = CH_2; R = H
II Z = CH_2, O; R = H
III Z = O; R = H
VI Z = O; R = –CO_2Et

Ia
IIa
IIIa
IVa

Scheme 1.

Despite the protection of the empty coordination place in the parent pentacoordinate complexes **I**–**III** by bulky *tert*-butyl groups [14], ^{t}BuNC coordination occurs *trans* to hydride ligand. This has very minor effect on the geometry of bonds in the plane involving pincer ligand (Ir-arene), leading to a small elongation of Ir–P and Ir–C_{ipso} bonds (<0.03 Å) as well as of Ir–Cl bonds (by ca. 0.06 Å, Table 3). C=N bonds lengths are within those reported for diverse Ir–C=N–^{t}Bu complexes found in CSD and decrease only slightly from **Ia** to **IIa** ≈ **IIIa**, while Ir–C_{CN} distance undergoes simultaneous increase. Similar to the parent **I**–**III**, in **Ia**–**IIIa** the CH protons of phosphorus bound *tert*-butyls are in the close proximity of chloride and hydride ligands with some distances being shorter than the corresponding sum of the van der Waals radii (2.4 Å for H...H, 3.0 Å for H...Cl). The coordinated isonitrile remains linear in **Ia**–**IIIa** and is

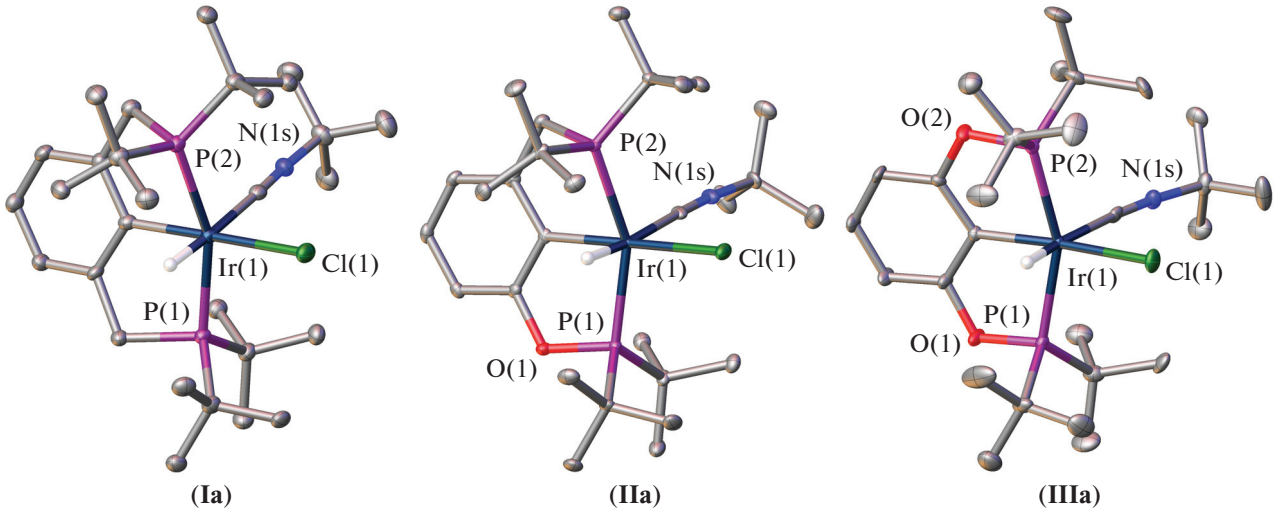

Fig. 1. General view of the complexes **Ia**–**IIIa**. Hydrogen atoms except those at the metal center are omitted for clarity, non-hydrogen atoms are shown as thermal ellipsoids at 30% probability level, and only heteroatoms are labelled.

Table 3. Selected bond lengths (Å) and angles (deg) for complexes **I**–**III** and **Ia**–**IIIa** from single-crystal X-ray diffraction data*

Bond	**I**	**Ia**	**II**	**IIa**	**III**	**IIIa**
	d, Å					
Ir–H	1.604	1.22(5)		1.39(5)	1.486	1.37(7)
Ir–Cl	2.425	2.484(2)	2.4012(10)	2.483(1)	2.404	2.469(2)
Ir–C_{ipso}	2.014	2.042(5)	2.016(3)	2.034(4)	2.01	2.005(6)
Ir–P(1)	2.305	2.327(1)	2.2685(9)	2.297(1)	2.293	2.329(2)
Ir–P(2)	2.305	2.317(2)	2.3194(8)	2.332(1)	2.297	2.322(2)
Ir–C_{CN}		2.012(6)		2.028(4)		2.031(7)
C=N		1.159(7)		1.150(6)		1.150(10)
N–C^{tBu}		1.454(8)		1.468(7)		1.48(1)
Angle	ω, deg					
HIrCl	89.44	102(2)		93(2)	99.94	85(3)
ClIrC_{ipso}	179.77	178.2(2)	177.71(9)	175.9(1)	179.12	171.9(2)
Ir–C=N (?)		177.5(5)		177.7(4)		172.6(7)
C_{ipso}IrC_{CN}		91.1(2)		93.8(2)		102.2(3)
NC inclination **		72.18(15)		77.64(17)		88.8(4)

* Deposition # – 757294, 728028 for **I**, **III**, respectivily; references [52], [23], [53] for **I**, **II**, **III**, respectively.
** Dihedral angle between arene–Ir and N=C–Ir–C_{ipso} planes.

almost orthogonal to the IrC_{ipso} bond in **Ia** with C_{ipso}IrC_{CN} angle increasing with introduction of oxygen bridges in **IIa** and **IIIa** (Table 3). This is probably a result of increased steric pressure from P–^{t}Bu groups as suggested by short CH...C_{CN} distances: the shortest distances from "left" and "right" P-^{t}Bu are 2.554(6), 2.662(5) Å in **Ia**, 2.461(5), 2.600(5) Å in **IIa**, 2.470(10), 2.483(9) Å in **IIIa**. In addition, C–H bonds of ^{t}BuNC exhibit short intermolecular contacts with arene ring of **IIa** (with CH...centroid distances of 2.361(6)–2.837(2) Å) or with chloride ligand of **IIIa** (with the shortest CH...Cl distance of 2.690(2) Å). Thus, the overall structural data suggest stronger binding of ^{t}BuNC to PCP-supported iridium center and weaker one for PCOP/POCOP species.

An important feature of pincer complexes is the geometry of P–M–P moiety. The rigidity of methylene bridges forces the deviation of both phosphorus atoms from the pincer ligand plane (involving arene ring and Ir atom) in **I**, while this tension is released upon introduction of oxygen bridges, making (POCOP)Ir moiety in **III** almost planar. At that isonitrile molecule is inclined relative to the arene–Ir plane increasing from **Ia** to **IIIa**, in which ^{t}BuNC is almost orthogonal to the pincer ligand plane. Docking ^{t}BuNC in apical position leads to a distortion of this fragment in each complex **Ia**–**IIIa** that is the most noticeable for asymmetric PCOP version **IIa**. Evaluated as a distance of P(2) atom to the plane P(1)–Ir–C_{ipso} it is the largest for non-symmetric **IIa**—0.668(2) Å in comparison to 0.592(3) Å for **Ia** and 0.400(5) Å for **IIIa**. This geometric distortion should lead to the deformation of iridium *d*-orbitals participating in Ir–P bonding and should thus affect the isonitrile binding by both the donation (C: → Ir) and the back-donation (Ir → C=N) channels.

In many instances the change of electrophilic character of the isonitrile's carbon and its ability to undergo nucleophilic attack is estimated measuring an increase of ν_{NC} vibration frequency upon the isonitrile coordination: $\Delta\nu_{NC} = \nu_{NC}^{bound} - \nu_{NC}^{free}$ [19]. To our surprise, in the IR spectra in CH_2Cl_2 the formation of (PCP)IrH(Cl)(CN^{t}Bu) complex **Ia** leads to the appearance of two new intense bands ν_1(**Ia**) = 2185 cm^{-1} (ε_1 = 480 M^{-1} cm^{-1}) and ν_2(**Ia**) = 2123 cm^{-1} (ε_2 = 500 M^{-1} cm^{-1}) instead of one ν_{NC} = 2139 cm^{-1} (230 M^{-1} cm^{-1}) of free ^{t}BuNC (Fig. 2). Their intensity increases in different extent with the temperature decrease, making the higher frequency band more intense (Fig. 3). Similar picture is observed in the solid state: in the IR spectrum of thin film the higher frequency band becomes even more asymmetric and has higher integral intensity (Fig. 4). Complexes **IIa**–**IVa** also exhibit in the solid state two bands of different relative intensity with low intensity lower frequency bands ν_2 partially overlapped with ν_1 (Fig. 4). In solution, the higher frequency asymmetric band splits in two, while the lower frequency band ν_1 remains the most intense showing the substantial intensity

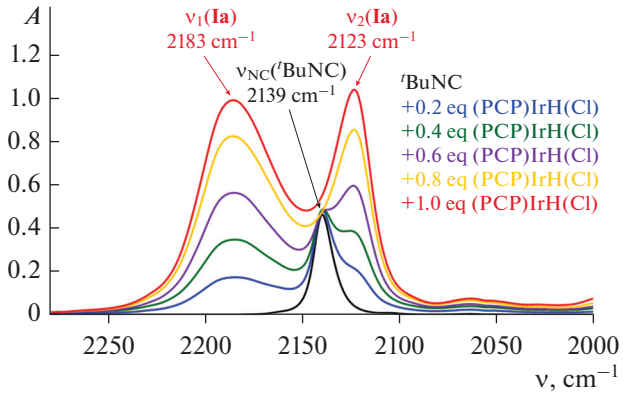

Fig. 2. IR spectra of ^{t}BuNC (0.04 M) in the presence of increasing amount of (PCP)IrH(Cl) (0.2–1 equiv.) at room temperature in CH_2Cl_2 (l = 0.05 cm).

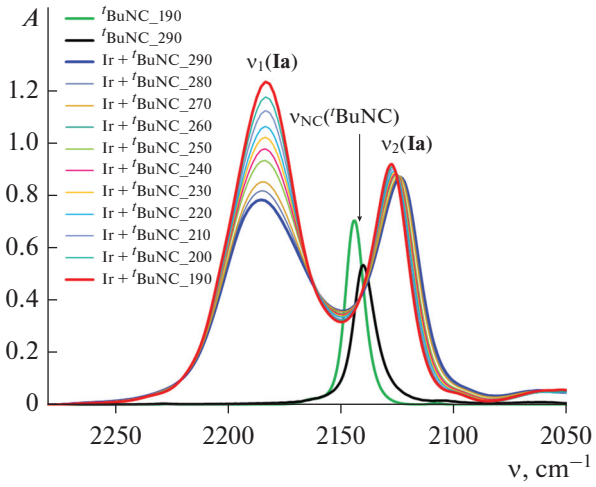

Fig. 3. Variable temperature IR spectra of ^{t}BuNC (0.02 M) and its complex (PCP)IrH(Cl)(CN^{t}Bu) (**Ia**), obtained in situ by the addition of equimolar amount of (PCP)IrH(Cl) (0.02 M) in CH_2Cl_2.

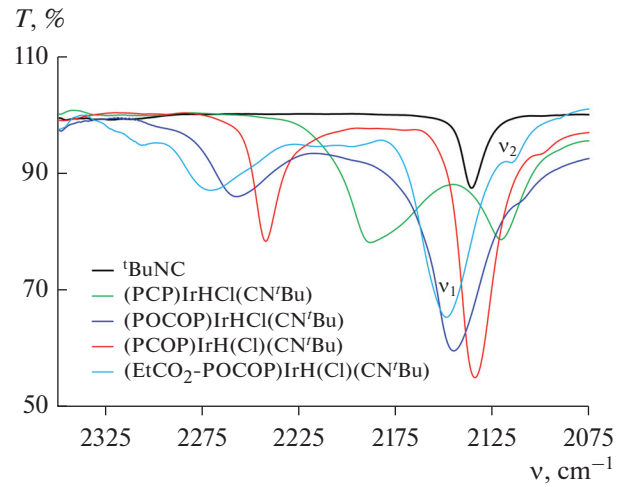

Fig. 4. Fragments of the IR spectra of ^{t}BuNC (neat) and its iridium complexes **Ia**–**IVa** in the solid state (thin films). ν_1 and ν_2 bands are shown on the example of **IVa** (sky blue line).

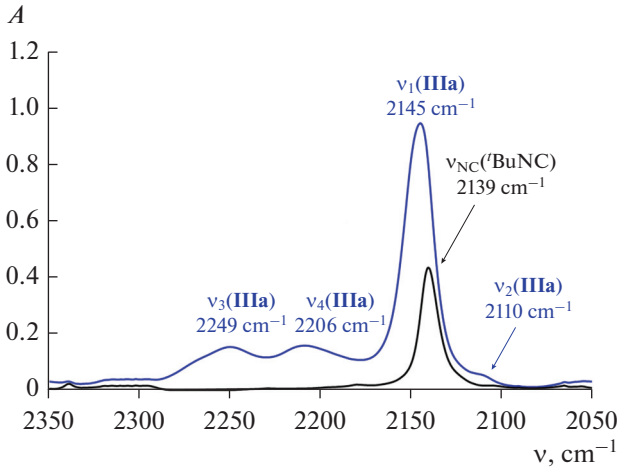

Fig. 5. IR spectra of ^{t}BuNC (0.02 M) and its complex (POCOP)IrH(Cl)(CN^{t}Bu) (**IIIa**), obtained *in* situ by the addition of equimolar amount of (POCOP)IrH(Cl) (**III**). Room temperature, CH_2Cl_2, l = 2.0 mm.

increase relative to $\nu_{N=C}$ of free ^{t}BuNC. For example, for complex **IIIa** in CH_2Cl_2 (Fig. 5) the strongest ν_1 band is observed at 2145 cm^{-1} (ε_1 = 470 M^{-1} cm^{-1}) overlapped with a low frequency ν_2 band at ~2110 cm^{-1} while the high frequency band observed in the solid state at 2258 cm^{-1} converts in solution into two bands of similar intensity (ε = 80 M^{-1} cm^{-1}) with maxima at ν_3 = 2249 and ν_4 = 2206 cm^{-1}. Such spectral picture suggests the strong vibrational coupling leading to the resonance intensity increase of N=C and Ir–H vibrations. Among the relevant literature examples of (PCP)IrH(X)(CN^{t}Bu) complexes the IR data are reported only for ($^{t\text{Bu}}$PCP)IrH(NH$_2$)(CN^{t}Bu) which also gives two vibrational bands in this region (2173, 2099 cm^{-1}) [48]. In an attempt to understand this phenomenon and make the bands assignment we performed the theoretical analysis of vibrational frequencies on the example of **Ia**.

DFT calculations of complex **Ia** were performed using two different approaches: method 1 was based on M06 functional to be compatible with that used previously to study hexacoordinate (PCP)IrH(Cl)L complexes with different ligands [15, 18], method 2 was B3PW91/def2-TZVP that should produce more reliable frequencies [54]. Both methods gave high

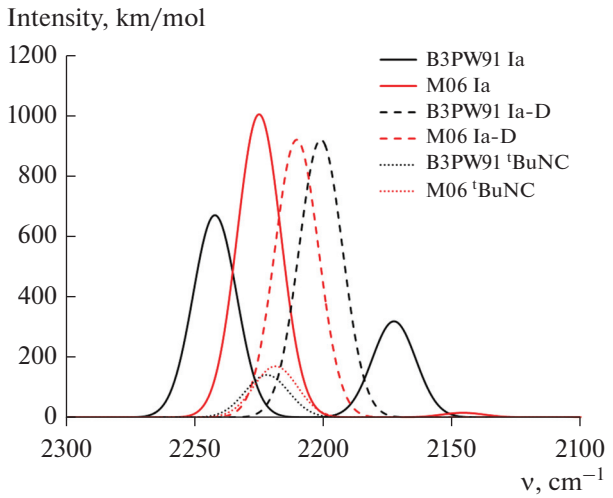

Fig. 6. IR spectra of (PCP)IrH(Cl)(CN^{t}Bu) complex (**Ia**; solid lines), its deuterated analogue (PCP)IrD-(Cl)(CN^{t}Bu) (**Ia–D**; dashed lines), and ^{t}BuNC (dotted lines) simulated using two different DFT methods (M06—red lines, B3PW91—black lines). FWHH was taken equal 20 cm^{-1}.

degree of vibrational coupling for ν_{Ir-H} and $\nu_{N=C}$ modes, but the intensities ratios obtained are quite different (Fig. 6). Method 1 gives low frequency of predominant Ir–H vibration ν_2 (43 : 17 Ir–H : R–N=C) with low intensity (2146 cm^{-1}, 15 km/mol) and high intensity for ν_1 band in which ν_{IrH} is highly mixed with NC stretching (23 : 38, 2225 cm^{-1}, 1006 km/mol). Method 2 shows larger influence of coordinate mixing on the intensities of IR bands, producing two bands of strongly coupled Ir–H/N=C vibrations, with corresponding coordinate impacts Ir–H : R–N=C 41 : 26 for ν_1 = 2242 cm^{-1} (671 km/mol) and 32 : 32 for ν_2 = 2173 cm^{-1} (319 km/mol). Additionally, we have checked decoupling of these vibrations upon H/D substitution, and it works exactly as it should. Substitution of hydridic hydrogen by deuterium leads to the only one band in the target region of N=C vibration with high intensity located between the two coupled Ir–H/N=C vibrations of the protic analogue (Fig. 6) even for low-degree-mixed vibrations obtained by method 1.

Based on the computational data we were compelled to assign the two bands, ν_1 and ν_2, observed in the experimental IR spectra of **Ia** to the equally mixed ν_{IrH} and ν_{NC} modes. Complexes **IIa–IVa** apparently show a low degree of vibrational coupling because of a weaker bonded isonitrile, and thus require another assignment. The strongest band ν_1 observed for **IIa–IVa** close to the ν_{NC}(^{t}BuNC) vibration is assigned to a mixed IrH/NC vibration. This band masks partially the low intensity low frequency band assigned to ν_{Ir-H} that becomes observable due to coupling with N=C stretch. At that higher frequency bands ν_3 and ν_4 (Fig. 5) appear to be a result of Fermi resonance that involves N=C and N–C$^{t\text{Bu}}$ bond fundamentals as well as their overtones and deformational vibrations [55]. Notably N–C$^{t\text{Bu}}$ bond is sensitive to the isonitrile coordination to Ir falling in the range 1.45–1.48 Å being the shortest in **Ia** (Table 3). This variation of the N–C$^{t\text{Bu}}$ bond can be important for its participation in Fermi resonance.

Overall this analysis suggests that the "true" ν_{NC} vibration should be located somewhere between ν_1 and ν_2 bands observed in the experimental IR spectra. As a rough estimate of correct ν_{NC} band position one could use a mean value $\nu' = (\nu_1 + \nu_2)/2$. For complexes **Ia–IVa** studied herein that changes from 2151 cm^{-1} for **Ia** to 2117–2131 cm^{-1} for **IIa–IVa**, with the corresponding $\Delta\nu_{N=C}$ going from positive value (+16 cm^{-1}) indicating a bond activation [19] to negative values equal −19, −8, −4 cm^{-1} for complexes **IIa–IVa** containing oxygen bridge(s) in the pincer ligand. This order **Ia** > **IVa** > **IIIa** is in agreement with the experimentally determined enthalpies of pyridine and benzonitrile binding to symmetric ($^{t\text{Bu}}$PZCZP)IrH(Cl) complexes [15].

CONCLUSIONS

Aliphatic isonitriles are shown being excellent σ-donors, good π-donors, and poor π-acceptors [56]. Having a large dipole moment with negative charge on the terminal carbon atom they are strong nucleophiles but their coordination to electrophilic (Lewis acidic) metal centers alters their reactivity. As the result of the charge redistribution entailed by coordination to transition metals, RN=C bonds become activated and prone even to the nuclephilic attack. The results of our study on the complexation of a series of iridium hydrido chlorides supported by benzene-based pincer ligands, ($^{t\text{Bu}}$PZCZP)IrH(Cl) (Z = CH_2, O), with ^{t}BuNC reveal that strong binding does not lead to a strong activation. The complexes form instantaneously and quantitatively upon the mixing ^{t}BuNC and ($^{t\text{Bu}}$PZCZP)IrH(Cl) in solution. Single crystal X-ray diffraction studies confirmed the formation of one isomer with apical coordination of isonitrile ligand *trans* to hydride ligand suggested by NMR studies. They also show shorter N=C and Ir–C_{CN} bond distances in complex **Ia** suggesting stronger binding of ^{t}BuNC to PCP-supported iridium center in comparison to PCOP/POCOP species **IIa–IIIa**. Structural data also reveal a distortion in the P–Ir–P arrangement caused by ^{t}BuNC docking in apical position that is the most noticeable for asymmetric PCOP version **IIa**. This geometric distortion should definitely lead to the deformation of iridium *d*-orbitals and affect

metal–isonitrile electronic communication. That, in turn, affects the IR spectral picture observed. However, the calculations suggest that raw experimental IR data should be taken with care as an indicator of RN=C activation, paying attention to the vibrational coupling. Coordination of a strong *trans* ligand is known to increase the intensity of metal-hydride stretching vibrations due to a vibrational coupling [57, 58]. Herein it leads to an essential coupling ν_{Ir-H} and $\nu_{N=C}$ modes that produce two strong bands of similar intensity in the $\nu_{N=C}$ region for **Ia**. Weaker isonitrile binding in **IIa**–**IVa** with shorter N=C and longer N–$C^{^tBu}$/Ir–C_{CN} bonds and a plethora of intramolecular interactions result in a different degree of vibrational mixing for Ir–H and N=C stretches as well as lead to an intense bands due to a Fermi resonance of low frequency modes involving vibrations of N–C–^{t}Bu fragment. An estimation of band position for the "true" (uncoupled) ν_{NC} vibration gives a small high frequency shift for **Ia** but low frequency shifts for other complexes becoming less negative in the order **IIa**–**IIIa**–**IVa** (PCOP–POCOP–$EtCO_2$-POCOP).

FUNDING

This work was financially supported by the Russian Science Foundation (grant no. 19-13-00459). X-ray diffraction data were collected using the equipment of Center for molecular composition studies of INEOS RAS with the financial support from Ministry of Science and Higher Education of the Russian Federation (Contract/agreement no. 075-03-2023-642).

CONFLICT OF INTEREST

The authors of this work declare that they have no conflicts of interest.

REFERENCES

1. *Pincer Compounds: Chemistry and Applications,* Morales-Morales, D., Ed., Amsterdam (Netherlands): Elsevier, 2018.
2. Kumar, A., Bhatti, T.M., and Goldman, A.S., *Chem. Rev.*, 2017, vol. 117, p. 12357. https://doi.org/10.1021/acs.chemrev.7b00247
3. Kumar, A. and Goldman, A.S., in *The Privileged Pincer-Metal Platform: Coordination Chemistry & Applications*, van Koten, G., Gossage, R.A., Eds., Cham: Springer Intern., 2016, p. 307.
4. Belkova, N.V., Filippov, O.A., Osipova, E.S., et al., *Coord. Chem. Rev.*, 2021, vol. 438, p. 213799. https://doi.org/10.1016/j.ccr.2021.213799
5. Prakasham, A.P., Vigalok, A., and Vedernikov, A.N., *Organometallics*, 2022, vol. 41, p. 634. https://doi.org/10.1021/acs.organomet.1c00710
6. Polukeev, A.V., Abdelaziz, O.Y., and Wendt, O.F., *Organometallics*, 2022, vol. 41, p. 859. https://doi.org/10.1021/acs.organomet.2c00012
7. Haibach, M.C., Kundu, S., Brookhart, M., and Goldman, A.S., *Acc. Chem. Res.*, 2012, vol. 45, p. 947. https://doi.org/10.1021/ar3000713
8. Choi, J., MacArthur, A.H.R., Brookhart, M., and Goldman, A.S., *Chem. Rev.*, 2011, vol. 111, p. 1761. https://doi.org/10.1021/cr1003503
9. Morales-Morales, D., Redon, R., Yung, C., and Jensen, C.M., *Inorg. Chim. Acta.*, 2004, vol. 357, p. 2953. https://doi.org/10.1016/j.ica.2004.01.033
10. Wang, Z., Belli, J., and Jensen, C.M., *Faraday Discuss.,* 2011, vol. 151, p. 297. https://doi.org/10.1039/C1FD00002K
11. Ahuja, R., Punji, B., Findlater, M., et al., *Nat. Chem.*, 2011, vol. 3, p. 167. https://doi.org/10.1038/nchem.946
12. Gu, X.Q., Chen, W., Morales-Morales, D., et al., *J. Mol. Catal. A*, 2002, vol. 189, p. 119. https://doi.org/10.1016/S1381-1169(02)00200-5
13. Dietrich, B.L., Goldberg, K.I., Heinekey, D.M., et al., *Inorg. Chem.*, 2008, vol. 47, p. 8583. https://doi.org/10.1021/ic801161g
14. Osipova, E.S., Filippov, O.A., Shubina, E.S., and Belkova, N.V., *Mendeleev. Commun.*, 2019, vol. 29, p. 121. https://doi.org/10.1016/j.mencom.2019.03.001
15. Osipova, E.S., Gulyaeva, E.S., Filippov, O.A., et al., *Eur. J. Inorg. Chem.*, 2019, vol. 2019, p. 1389. https://doi.org/10.1002/ejic.201801341
16. Segawa, Y., Yamashita, M., and Nozaki, K., *J. Am. Chem. Soc.*, 2009, vol. 131, p. 9201. https://doi.org/10.1021/ja9037092
17. Titova, E.M., Silantyev, G.A., Filippov, O.A., et al., *Eur. J. Inorg. Chem.*, 2016, p. 56. https://doi.org/10.1002/ejic.201501083
18. Titova, E.M., Osipova, E.S., Gulyaeva, E.S., et al., *J. Organomet. Chem.*, 2017, vol. 827, p. 86. https://doi.org/10.1016/j.jorganchem.2016.11.010
19. Michelin, R.A., Pombeiro, A.J.L., and Guedes da Silva, M.F.C., *Coord. Chem. Rev.*, 2001, vol. 218, p. 75. https://doi.org/10.1016/S0010-8545(01)00358-7
20. Boyarskiy, V.P., Bokach, N.A., Luzyanin, K.V., and Kukushkin, V.Y., *Chem. Rev.*, 2015, vol. 115, p. 2698. https://doi.org/10.1021/cr500380d
21. Boyarskiy, V.P., Luzyanin, K.V., and Kukushkin, V.Y., *Coord. Chem. Rev.*, 2012, vol. 256, p. 2029. https://doi.org/10.1016/j.ccr.2012.04.022
22. Krogh-Jespersen, K., Czerw, M., Zhu, K., et al., *J. Am. Chem. Soc.*, 2002, vol. 124, p. 10797. https://doi.org/10.1021/ja010547t
23. Nawara-Hultzsch, A.J., Hackenberg, J.D., Punji, B., et al., *ACS Catal.*, 2013, vol. 3, p. 2505. https://doi.org/10.1021/cs400624c
24. Göttker-Schnetmann, I. and Brookhart, M., *J. Am. Chem. Soc.*, 2004, vol. 126, p. 9330. https://doi.org/10.1021/ja048393f
25. Polukeev, A.V., Kuklin, S.A., Petrovskii, P.V., et al., *Russ. Chem. Bull.*, 2010, vol. 59, p. 745. https://doi.org/10.1007/s11172-010-0156-6
26. Sheldrick, G., *Acta Crystallogr., Sect. A: Found. Adv.*, 2015, vol. 71, p. 3. https://doi.org/10.1107/S2053273314026370

27. Dolomanov, O.V., Bourhis, L.J., Gildea, R.J., et al., *J. Appl. Crystallogr.*, 2009, vol. 42, p. 339. https://doi.org/10.1107/S0021889808042726

28. Sheldrick, G., *Acta Crystallogr., Sect. A: Found. Cryst.*, 2008, vol. 64, p. 112. https://doi.org/10.1107/S0108767307043930

29. Frisch, M.J., Trucks, G.W., Schlegel, H.B., et al., *Gaussian 09, Revision B.1*, Gaussian, Inc.: Wallingford CT, 2009.

30. Zhao, Y. and Truhlar, D.G., *Theor. Chem. Acc.*, 2008, vol. 120, p. 215. https://doi.org/10.1007/s00214-007-0310-x

31. Becke, A.D., *Phys. Rev. A: At., Mol., Opt. Phys.*, 1988, vol. 38, p. 3098. https://doi.org/10.1103/physreva.38.3098

32. Becke, A.D.J., *Chem. Phys.*, 1993, vol. 98, p. 5648. https://doi.org/10.1063/1.464913

33. Silantyev, G.A., Filippov, O.A., Musa, S., et al., *Organometallics*, 2014, vol. 33, p. 5964. https://doi.org/10.1021/om500308g

34. Titova, E.M., Osipova, E.S., Pavlov, A.A., et al., *ACS Catal.*, 2017, vol. 7, p. 2325. https://doi.org/10.1021/acscatal.6b03207

35. Luconi, L., Osipova, E.S., Giambastiani, G., et al., *Organometallics*, 2018, vol. 37, p. 3142. https://doi.org/10.1021/acs.organomet.8b00488

36. Kirkina, V.A., Osipova, E.S., Filippov, O.A., et al., *Mendeleev Commun.*, 2020, vol. 30, p. 276. https://doi.org/10.1016/j.mencom.2020.05.004

37. Andrae, D., Häußermann, U., Dolg, M., et al., *Theor. Chim. Acta*, 1990, vol. 77, p. 123. https://doi.org/10.1007/bf01114537

38. Haussermann, U., Dolg, M., Stoll, H., et al., *Mol. Phys.*, 1993, vol. 78, p. 1211.

39. Kuchle, W., Dolg, M., Stoll, H., and Preuss, H.J., *Chem. Phys.*, 1994, vol. 100, p. 7535.

40. Leininger, T., Nicklass, A., Stoll, H., Dolg, M., and Schwerdtfeger, P.J., *Chem. Phys.*, 1996, vol. 105, p. 1052.

41. Ehlers, A.W., Bohme, M., Dapprich, S., et al., http://www.sciencedirect.com/science/article/B6TFN-44WCWM6-G7/2/de72037e161a580451f5f174ff0a7921.

42. Hehre, W.J., Ditchfield, R., and Pople, J.A.J., *Chem. Phys.*, 1972, vol. 56, p. 2257. https://doi.org/10.1063/1.1677527

43. Francl, M.M., Pietro, W.J., Hehre, W.J., et al., *J. Chem. Phys.*, 1982, vol. 77, p. 3654. https://doi.org/10.1063/1.444267

44. Clark, T., Chandrasekhar, J., Spitznagel, G.W., and Schleyer, P.V.R.J., *Comput. Chem.*, 1983, vol. 4, p. 294. https://doi.org/10.1002/jcc.540040303

45. Hariharan, P.C. and Pople, J.A., *Theoret. Chim. Acta.*, 1973, vol. 28, p. 213. https://doi.org/10.1007/bf00533485

46. Weigend, F. and Ahlrichs, R., *Phys. Chem. Chem. Phys.*, 2005, vol. 7, p. 3297. https://doi.org/10.1039/b508541a

47. Andrae, D., Häußermann, U., Dolg, M., et al., *Theor. Chim. Acta.*, 1990, vol. 77, p. 123. https://doi.org/10.1007/bf01114537

48. Kanzelberger, M., Zhang, X., Emge, T.J., et al., *J. Am. Chem. Soc.*, 2003, vol. 125, p. 13644. https://doi.org/10.1021/ja037363u

49. Zhang, X., Emge, T.J., Ghosh, R., et al., *Organometallics*, 2006, vol. 25, p. 1303. https://doi.org/10.1021/om050659j

50. Zhang, X., Emge, T.J., Ghosh, R., and Goldman, A.S., *J. Am. Chem. Soc.*, 2005, vol. 127, p. 8250. https://doi.org/10.1021/ja051300p

51. Huang, Z., Zhou, J., and Hartwig, J.F., *J. Am., Chem. Soc.*, 2010, vol. 132, p. 11458. https://doi.org/10.1021/ja1053835

52. Punji, B., Emge, T.J., and Goldman, A.S., *Organometallics.*, 2010, vol. 29, p. 2702. https://doi.org/10.1021/om100145q

53. Arunachalampillai, A., Olsson, D., and Wendt, O.F., *Dalton Trans.*, 2009, p. 8626. https://doi.org/10.1039/B910798C

54. Medel, R., Stelbrink, C., and Suhm, M.A., *Angew. Chem. Int. Ed.*, 2019, vol. 58, p. 8177. https://doi.org/10.1002/anie.201901687

55. Morgenstern, D.A., Ferrence, G.M., Washington, J., et al., *J. Am. Chem. Soc.*, 1996, vol. 118, p. 2198. https://doi.org/10.1021/ja953010m

56. Csonka, I.P., Szepes, L., and Modelli, A.J., *Mass Spectrom.*, 2004, vol. 39, p. 1456. https://doi.org/10.1002/jms.761

57. Jacobsen, H., Jonas, V., Werner, D., et al., *Helv. Chim. Acta*, 1999, vol. 82, p. 297. https://doi.org/10.1002/(SICI)1522-2675(19990210)82:2%3C297::AID-HLCA297%3E3.0.CO;2-Y

58. Shubina, E.S., Belkova, N.V., Krylov, A.N., et al., *J. Am. Chem. Soc.*, 1996, vol. 118, p. 1105. https://doi.org/10.1021/ja953094z